FFI RAPPORT

IONOSPHERIC INFLUENCE ON X-BAND RADIO SIGNALS

BLIX Tom Arild, SVENES Knut Ragnar, HOPPE Ulf-Peter

FFI/RAPPORT-2003/01761

FFIE/416001/172

Approved
Kjeller 23. May 2003

Vidar S Andersen
Director of Research

IONOSPHERIC INFLUENCE ON X-BAND RADIO SIGNALS

BLIX Tom Arild, SVENES Knut Ragnar, HOPPE Ulf-Peter

FFI/RAPPORT-2003/01761

FORSVARETS FORSKNINGSINSTITUTT
Norwegian Defence Research Establishment
P O Box 25, NO-2027 Kjeller, Norway

FORSVARETS FORSKNINGSINSTITUTT (FFI)
Norwegian Defence Research Establishment

P O BOX 25
N0-2027 KJELLER, NORWAY

UNCLASSIFIED

SECURITY CLASSIFICATION OF THIS PAGE
(when data entered)

REPORT DOCUMENTATION PAGE

1) PUBL/REPORT NUMBER	2) SECURITY CLASSIFICATION	3) NUMBER OF PAGES
FFI/RAPPORT-2003/01761	UNCLASSIFIED	23
1a) PROJECT REFERENCE	**2a) DECLASSIFICATION/DOWNGRADING SCHEDULE**	
FFIE/416001/172	-	

4) TITLE

IONOSPHERIC INFLUENCE ON X-BAND RADIO SIGNALS

5) NAMES OF AUTHOR(S) IN FULL (surname first)

BLIX Tom Arild, SVENES Knut Ragnar, HOPPE Ulf-Peter

6) DISTRIBUTION STATEMENT

Approved for public release. Distribution unlimited. (Offentlig tilgjengelig)

7) INDEXING TERMS

IN ENGLISH:	IN NORWEGIAN:
a) Ionosphere	a) Ionosfære
b) Scintillations	b) Scintillasjoner
c) Satellite navigation	c) Satellittnavigasjon
d) Geolocation	d) Lokalisering
e) Aurora	e) Nordlys

THESAURUS REFERENCE:

8) ABSTRACT

We systematically study the possible effects of the ionosphere on radiowave propagation in the X-band. The quiet ionosphere and various types of ionosphere disturbance are considered. We place special emphasis on high latitudes. For the viewing geometry that we study, we find the worst case deviation 35-50 m, as long as the viewing angle is no more than 65° from nadir. The polarisation, or phase, is modified by less than 0.03° by the complete path transmitter-receiver.

9) DATE	AUTHORIZED BY	POSITION
	This page only	
23. May 2003	Vidar S Andersen	Director of Research

ISBN 82-464-0724-4

UNCLASSIFIED

SECURITY CLASSIFICATION OF THIS PAGE
(when data entered)

CONTENTS

		Page
1	INTRODUCTION	7
2	IONOSPHERIC ELECTRON DENSITY, REFRACTIVE INDEX, AND ELECTROMAGNETIC WAVES	7
2.1	Basic description	8
2.2	Radio wave polarization changes	11
2.3	Problems caused by ionospheric irregularities	11
3	THE QUIET IONOSPHERE: ELECTRON DENSITY AS A FUNCTION OF SOLAR ELEVATION, SOLAR CYCLE, AND ALTITUDE	12
3.1	International Reference Atmosphere (IRI)	12
3.2	Extreme cases	13
4	THE DISTURBED IONOSPHERE AT HIGH LATITUDES	16
4.1	Aurora and particle precipitation	17
4.2	Polar cap irregularities	19
4.3	Polar Cap Absorption events (PCA)	20
5	SUMMARY AND CONCLUSIONS	21
	References	22
	Distribution list	23

IONOSPHERIC INFLUENCE ON X-BAND RADIO SIGNALS

1 INTRODUCTION

In most space-based navigation applications (GPS, GLONASS, or similar) the ionospheric influence potentially modifies the results through a difference between the geometric (Euclidian) path and the "optical" (radiowave) path, i.e. through the modifications to the path length due to the refractive index. Such influences have been addressed by, for instance, Schlüter et al. (2002). The next order correction is due to small-scale variation of the refractive index between the satellite and the receiver, or due to fast variations in time of this refractive index. These are called scintillations and have most recently been addressed by Basu et al. (2002). At FFI, these effects have been studied by Ofstad et al. (1991). Both effects are currently being studied in light of ESA's planned navigation system Galileo (Hoppe, 2002). As is described by Hoppe (2002), the influence of ionospheric scintillations on space-based radionavigation is so serious, that the U.S. will launch a dedicated satellite to forecast scintillations (See also FFI-Rapport - 2002/03188, that gives an introduction to space weather).

The present report deals with another side of this problem: Here, we are not interested in the path length modifications due to the ionosphere, but to the modifications of angle of arrival at a satellite. When "imaging" radio sources on the Earth's surface in the X-band from a space platform, do the sources seem to be displaced sideways compared to their true location? We estimate this effect, and show that it can be neglected.

2 IONOSPHERIC ELECTRON DENSITY, REFRACTIVE INDEX, AND ELECTROMAGNETIC WAVES

The presence of the ionosphere will impose variations of the refractive index with height. The effects from an undisturbed atmosphere will be systematic, and can therefore be compensated if necessary, while irregularities in space and time may cause stochastic variations. The ionospheric effects (on radio waves) are generally not large at frequencies greater than about 30 MHz, i.e. for frequencies above the HF band. Although it is small, we have estimated the deflection and phase distortion of the wave at the actual frequency of f=9.4 GHz. The program we have developed for this purpose can also be applied to other frequencies (e.g. GPS frequencies). The most important effects can be summarized in the following three points:

1. The wave will be refracted when it travels through the ionosphere, due to the vertical variation of the electron content.

2. Refractive index irregularities in the medium can cause different radio paths (wave velocity) and thereby distort the phase front in space and time.

3. Scintillations may occur, e.g. when the radio wave passes through auroral structures.

2.1 Basic description

The complex refractive index of the ionosphere can be written as:

$$n^2 = (\mu - ix)^2 \tag{2.1}$$

where the real part represent the phase and the imaginary part the absorption. In the general case the Appleton-Hartree formula, describing the propagation and characteristics of a wave in a magnetoionic medium can be written as:

$$n^2 = 1 - \frac{X}{1 - iZ - \left[{Y_T}^2 / 2(1 - X - iZ)\right] \pm \sqrt{{Y_T}^4 / 4(1 - X - iZ)^2 + {Y_L}^2}} \tag{2.2}$$

Where X, Y and Z are defined as:

$$X = \frac{{\omega_{pe}}^2}{\omega^2} \qquad Y = \frac{\omega_{ce}}{\omega} \qquad Z = \frac{\nu_{en}}{\omega} \tag{2.3a,b,c}$$

Y_L and Y_T are defined as $Y_L = Y\cos\theta$ and $Y_T = Y\sin\theta$ (θ being the angle between the wave vector **k** and the magnetic field vector $\mathbf{B_0}$), respectively. Here, ω is the angular wave frequency of the transmitted wave, and ω_{pe}, ω_{ce} and ν_{en} are the electron plasma frequency, the electron gyro frequency and the electron-neutral collision frequency, respectively. These can be expressed as:

$${\omega_{pe}}^2 = \frac{N_e e^2}{\varepsilon_0 m_e} \qquad \omega_{ce} = \frac{eB_0}{m_e} \qquad \nu_{en} = (1.43 + 2.76/\sqrt{T})10^8 P \tag{2.4 a,b,c}$$

The different symbols/parameters in the above expression have the following definition: N_e is the electron number density in m^{-3}, e is the elementary charge, ε_0 is the permittivity of free space, m_e is the electron mass, B_0 is the Earth's magnetic field, T is the atmospheric temperature in K and P is the atmospheric pressure in mbar.

ω_{pe} varies with height because of the dependence upon the electron number density. As will be shown below, the electron density will not be much larger than 10^{13} m^{-3} below 600 km height. This means that at all heights considered in this investigations, $\omega_{pe} < 2\text{x}10^8$ rad/s. Depending upon the actual location (latitude and longitude) the magnetic field $B_0 < 50000$nT. The electron

gyro frequency will thus be less than $9x10^6$ rad/s. The electron-neutral collision frequency ν_{en} is directly proportional to the atmospheric pressure P that decreases almost monotonically with increasing height. In our calculations presented below, we neglect the ionosphere below about 70 km (N_e=0). At 70 km the pressure is about $5x10^{-2}$ mb. The temperature dependence on ν_{en} is not large and we may use a typical value of about 220 K at 70 km to estimate ν_{en}. We then find that at all heights considered in this study, $\nu_{en}<10^7$ Hz. We may then find upper values for the X, Y and Z parameters of the Appleton-Hartree formula. With a wave frequency of f=9.4 GHz ($\omega=5.9x10^{10}$ rad/s) we see that $X<10^{-5}$, $Y<1.5x10^{-4}$, and $Z<1.5x10^{-4}$. These small values mean that the denominator of Equation (2.2) can be approximated to 1. The real part of the refractive index at high frequencies can therefore be written:

$$\mu^2 = \quad 1 - X = \quad 1 - \frac{\omega_{pe}^2}{\omega^2} \tag{2.5}$$

This equation can also be expressed as:

$$\mu^2 \approx 1 - \frac{81 \cdot N_e}{f^2} \tag{2.6}$$

where f is the wave frequency in Hz and N_e the electron density in m^{-3}. For a given electron density profile we can thus compute the refractive index as a function of height.

The refraction of a wave results in an error in the location of the radio source. The refraction is given by Snell's law:

$$\mu_i \sin\theta_i = \mu_r \sin\theta_r \tag{2.7}$$

Here, μ_i and μ_r are the refractive indices above and below the refraction height, and θ_i and θ_r are the angle of incidence and the angle of refraction, respectively. Figure 2.1 describes the situation for *one* refraction height only, but we can find the total refraction through the ionosphere by adding the individual refractions for a given electron density height profile.

The program we have developed uses a height resolution of 10 km between the ground and the satellite altitude (600 km). We have applied several realistic electron density profiles in this study in order to examine typical and worst case scenarios of wave propagation. The results are presented in different sub-chapters of this report treating these examples separately.

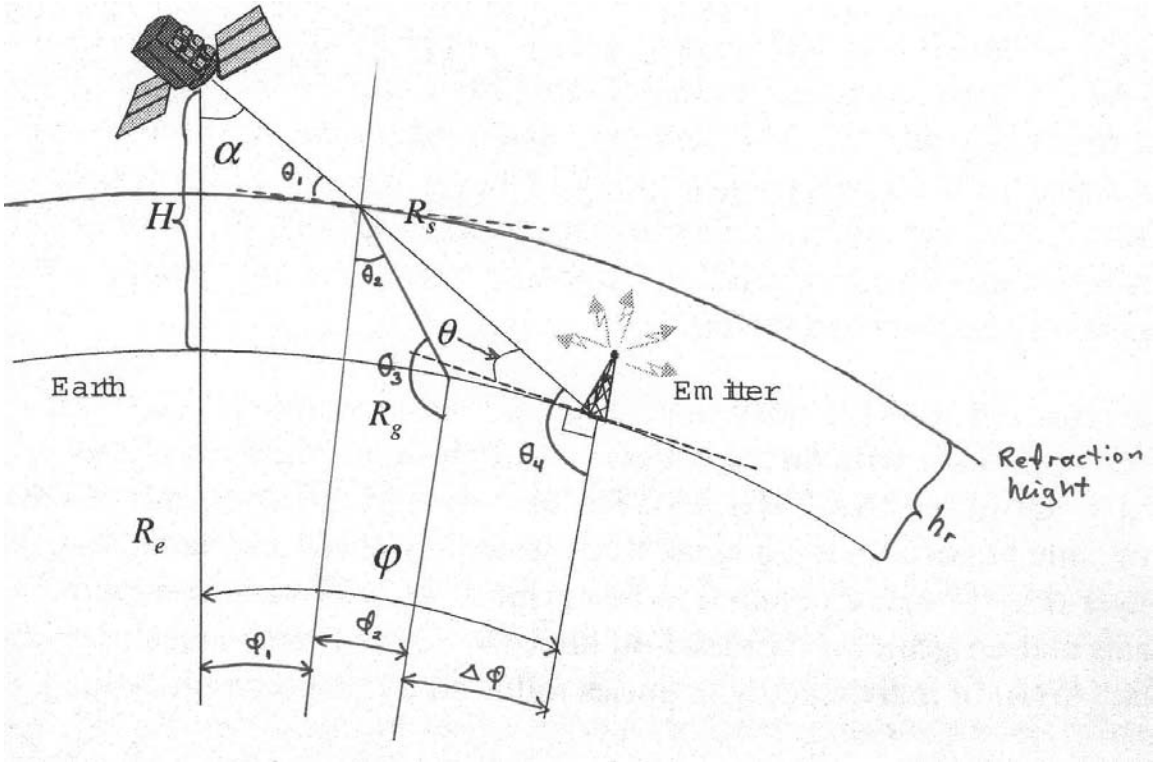

Figure 2.1. Geometry of wave propagation between the transmitter (on the ground) and the satellite at 600 km height. See text for further details.

The geometry of the method we have applied to investigate the effect of refraction is, as already said, shown in Figure 2.1. For each individual refraction height h_r, we calculate the angular change φ_i. We then find the total angular change (along the surface of the Earth; given by φ in Figure 2.1) by adding the individual change for each height step of 10 km ($\varphi_1+\varphi_2+\varphi_3+\ldots$). The uncertainty in the position of the transmitter can then be found as the difference between the direct line of sight from the satellite to the receiver along the surface of the Earth and the calculated position taken the ionosphere into account. The angular uncertainty of the position is therefore given as:

$$\Delta\varphi = \varphi - \sum_i \varphi_i \tag{2.8}$$

This angular uncertainty can be translated to a length uncertainty L by:

$$L = R_E \Delta\varphi \tag{2.9}$$

Where R_E is the Earth's average radius (6371 km) and $\Delta\varphi$ is given in radiances (rad).

2.2 Radio wave polarization changes

Another effect that may cause problems is changes of the polarization of the wave due to propagation through the ionosphere. Using the same nomenclature as in the last section we may express the resulting angular change of the wave as:

$$d\Omega = \tfrac{1}{2}\frac{\omega}{c}\frac{XY_L(1-Y_L{}^2-Z^2)}{\left[Z^2+(1-Y_L)^2\right]\left[Z^2+(1+Y_L)^2\right]}ds \tag{2.10}$$

where c is the speed of light and ds a length along the path of propagation. As shown previously, X, Y and Z are very small (<<1), such that Equation (2.10) can be approximated by:

$$d\Omega = \tfrac{1}{2}\frac{\omega}{c}XY_L ds \tag{2.11}$$

The maximum path of propagation is close to 3000 km for the worst-case viewing angle of 66°. The maximum dΩ is thus, using the values for X and Y found in the previous section, about $5\text{x}10^{-4}$ rad (0.03°). This is insignificant: The transmitted wave with frequency 9.4 GHz will preserve its wave polarization travelling through the ionosphere. For comparison, at GPS frequencies (1.2 GHz) the polarization change may be as large as 0.227 rad (13°). However, this estimate assumes that the electron density is as large as 10^{13} m^{-3} in the complete height range (600 km in our case). We therefore conclude that polarization changes should not cause any problems.

2.3 Problems caused by ionospheric irregularities

Another problem that can affect the performance is due to ionospheric irregularities that can have many sources. In the extreme case we may assume that the ionospheric column between the satellite and the "bottom" of the ionosphere is filled with such irregularities. The spatial extent of these irregularities depends very much upon the actual situation and the type of irregularity. At least 10% variation of the plasma density has been measured over scales of about 2-3 m. We are interested in scales of typically 25 cm, since this is the distance between the two antennas on the satellite. Ionospheric irregularities at such scales do also exist, but will be smaller than 10% as mentioned above. We can, as examples, calculate the effect for 1% and 0.1% fluctuations to illustrate the situation.

With a background plasma density of 10^{12} m^{-3}, a 1% variation corresponds to an absolute density variation of 10^{10} m^{-3}. Again we can use the same geometry to illustrate the worst-case scenario. The path through the ionosphere will in this case be approximately 1550 km. In such a column it is, statistically speaking, possible to have about $6.2\text{x}10^6$ "blobs" of plasma with a

dimension of 25 cm. The standard deviation of this number is 2490. We may therefore assume that there are about 2500 more (or less) blobs in one column than another between the satellite and the bottom of the ionosphere. Each of these blobs will cause a phase delay between the two paths to the antennas onboard the satellite. This effect can be calculated from the following expression, which describes the relation between the indices of refraction and the wavelengths inside and outside of the blob:

$$\mu_1\lambda_1 = \mu_2\lambda_2 \tag{2.12}$$

where the indices 1 and 2 describe the situation inside and outside of the blob, respectively. With a 1% and a 0.1% fluctuation, we find that the one blob will cause a difference in wavelength of 1.1 nm and 0.11 nm, in these two cases. This corresponds to phase differences of 0.000013° and 0.0000013°, respectively. With about 2500 blobs difference between the two paths, this gives a total difference of 2.75 μm and 0.275 μm. The phase difference will be 0.033° and 0.0033°, respectively. Consequently, ionospheric irregularities should not cause any significant problems at the chosen frequency of 9.4 GHz.

3 THE QUIET IONOSPHERE: ELECTRON DENSITY AS A FUNCTION OF SOLAR ELEVATION, SOLAR CYCLE, AND ALTITUDE

3.1 International Reference Atmosphere (IRI)

The quiet ionosphere is best represented by a standard model recommended by both the Committee On Space Research (COSPAR) and the International Union of Radio Science (URSI). The latest version, the International Reference Ionosphere (IRI) 2000, is described in Bilitza (2001) and references therein. The model specifies ionospheric densities and temperatures as function of altitude and latitude on the basis of coupled physical and statistical representations of the various ionospheric regions. External drivers like daily and seasonal variations in total solar irradiation as well as solar cycle activity are also taken into account.

An implementation of the IRI-2000 model can be found at the website: http://nssdc.gsfc.nasa.gov/space/model/models_home.html. This version has been used to produce the summary presented in table 3.1 below. The table shows the peak density and corresponding altitude as function of latitude for day and night conditions during both a solar maximum and minimum situation. These results describe the ionospheric conditions during (geomagnetically) quiet times in the regions relevant for observations from NSAT-1.

As is seen from the table, the F2-peak is always present. It is stronger at low latitudes than at high, and it is also stronger during solar maximum than minimum (when the peak altitude is also considerably lower). This peak is also stronger during daytime than night (when the peak

altitude is higher). The F1-peak is only present when the ionosphere is sunlit, hence usually only in daytime except at very high latitudes. This peak is also stronger during solar maximum then minimum, and it usually occurs about 100 km below the F2-peak. The E-layer is always present, but it is very weak in a dark ionosphere (roughly about a factor of 10 lower in density). The E-layer is also a bit stronger at solar maximum than at solar minimum.

	SOLAR MINIMUM				**SOLAR MAXIMUM**			
	NIGHT		**DAY**		**NIGHT**		**DAY**	
Latitude	H (km)	D(cm^{-3})	H (km)	D(cm^{-3})	H (km)	D(cm^{-3})	H (km)	D(cm^{-3})
55° W	316	$0.7\cdot10^5$	214	$2.8\cdot10^5$	373	$1.9\cdot10^5$	283	$1.8\cdot10^6$
55° S F2	301	$1.8\cdot10^5$	224	$2.9\cdot10^5$	379	$5.9\cdot10^5$	321	$7.7\cdot10^5$
F1			182	$2.3\cdot10^5$			213	$3.9\cdot10^5$
E			110	$1.2\cdot10^5$			110	$1.8\cdot10^5$
65° W	316	$5.3\cdot10^4$	228	$1.6\cdot10^5$	377	$2.4\cdot10^5$	288	$1.3\cdot10^6$
65° S F2	287	$1.7\cdot10^5$	235	$2.7\cdot10^5$	363	$4.7\cdot10^5$	319	$6.2\cdot10^5$
F1			192	$2.1\cdot10^5$			218	$3.5\cdot10^5$
E			110	$1.1\cdot10^5$			110	$1.6\cdot10^5$
75° W	315	$4.8\cdot10^4$	255	$8.4\cdot10^4$	374	$3.3\cdot10^5$	307	$7.2\cdot10^5$
75° S F2	271	$1.8\cdot10^5$	249	$2.6\cdot10^5$	340	$4.1\cdot10^5$	322	$5.2\cdot10^5$
F1			205	$1.9\cdot10^5$			224	$3.0\cdot10^5$
E			110	$9.6\cdot10^4$			110	$1.4\cdot10^5$
85° W	317	$7.4\cdot10^4$	284	$7.7\cdot10^4$	366	$3.9\cdot10^5$	331	$3.6\cdot10^5$
85° S F2	275	$2.1\cdot10^5$	257	$2.2\cdot10^5$	335	$4.0\cdot10^5$	324	$4.6\cdot10^5$
F1	233	$1.6\cdot10^5$	218	$1.8\cdot10^5$	234	$2.3\cdot10^5$	224	$2.6\cdot10^5$
E	110	$6.3\cdot10^4$	110	$7.7\cdot10^4$	110	$8.9\cdot10^4$	110	$1.1\cdot10^5$

Keys: W = Winter and S = Summer. The E-layer altitude is assumed to be 110 km always.

Table 3.1. Summary of peak electron densities and corresponding altitudes for the ionospheric E-layer and F-layer.

The highest density seen in this model is $n_e = 2\cdot 10^6\ cm^{-3}$ at 283 km altitude. This occurs in daytime during the winter at low latitude during solar maximum. The F2-peak maximum altitude is 379 km at night during solar maximum.

3.2 Extreme cases

We have investigated the effects of the ionosphere for solar maximum and minimum and for winter and summer, respectively. The profiles are shown in the figures below.

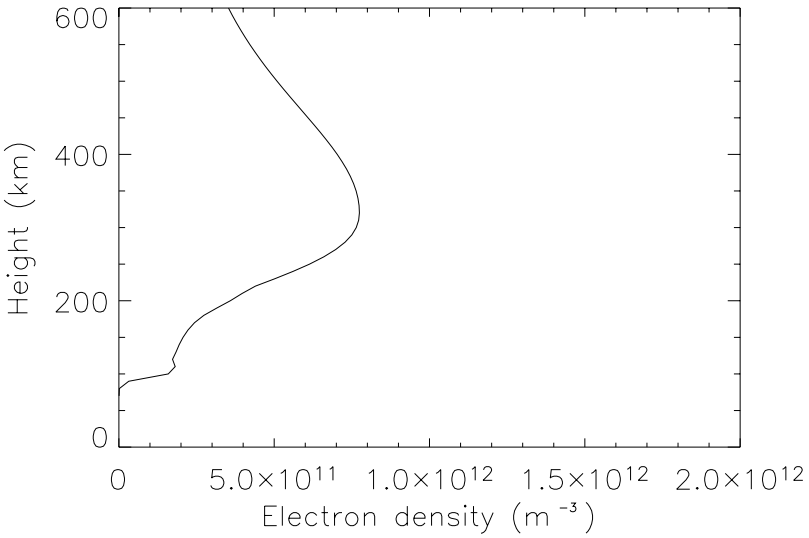

Figure 3.1. Electron density profile for solar maximum and summer conditions.

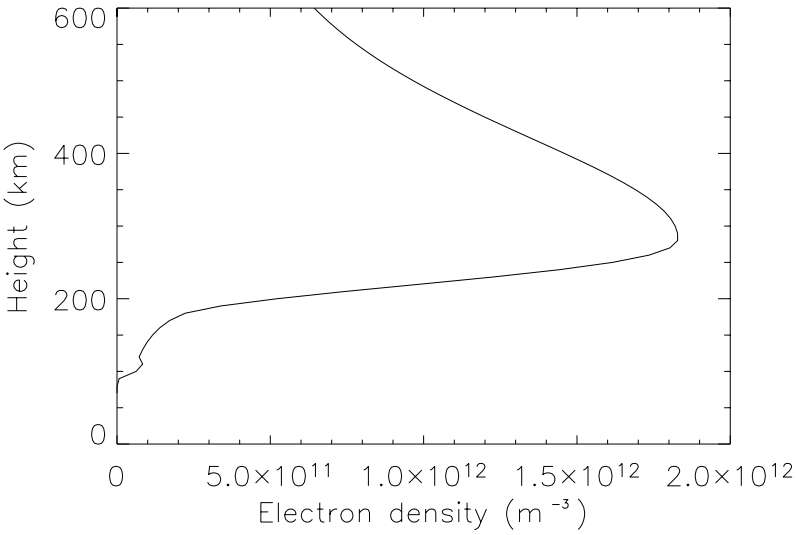

Figure 3.2. Electron density profile for solar maximum and winter conditions.

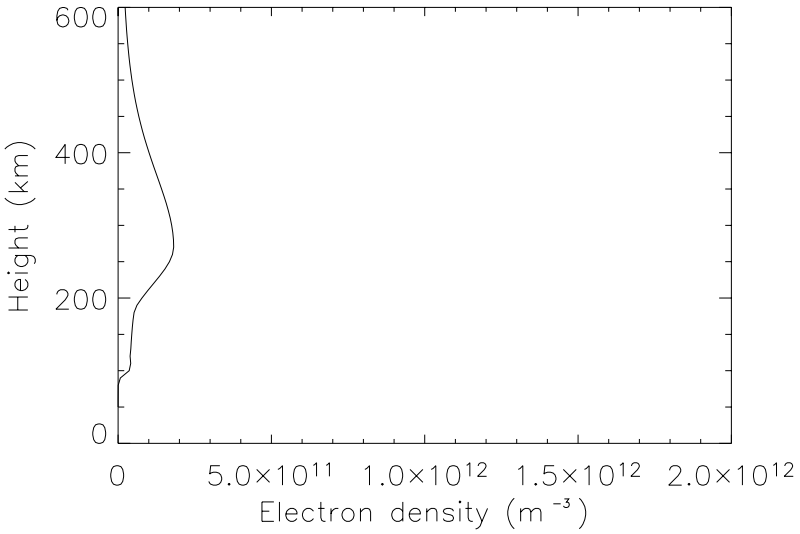

Figure 3.3. Electron density conditions for solar minimum and summer conditions.

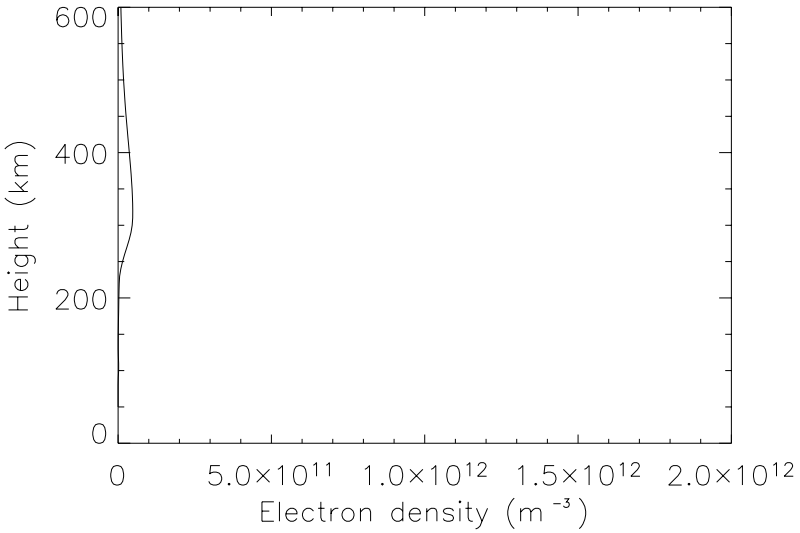

Figure 3.4. Electron density profile for solar minimum and winter conditions.

The four different profiles have been used as input to the model described in Section 2 to investigate the effect of the ionosphere upon radio-wave transmission in the X-band. We have concentrated on the worst-case scenario, i.e. 65° angle of reception with respect to nadir at the satellite height. We find that in all the four cases the deviation of the wave caused by the ionosphere is in the range 35-50 m. The largest value is found for solar maximum during winter (largest peak electron density). The deviation will decrease with decreasing angle of reception. For example, for 60° reception the deviation is in the range 15-25 m. For an angle of 66° (close to absolute maximum) the deviation is 120 m and 210 m for summer and winter

conditions during solar maximum. From this we conclude that for all practical purposes, the deviation in the position of the transmitter (on the ground) is less than 50 m seen from the satellite.

4 THE DISTURBED IONOSPHERE AT HIGH LATITUDES

Ionospheric disturbances at high latitudes are dependent on solar activity. This activity, which is often represented by variation in number of sunspots, varies in a cycle of roughly 11 years duration. In figure 4.1 the last few solar cycles are plotted by variations in sunspot number as function of time. It is seen that the last peak occurred in 2001, but also that both the duration and intensity of the cycles changes considerably.

We consider three main sources of disturbances in this report: solar proton events (leading to PCA) – auroral activity (restricted to latitudes covered by the auroral oval) – polar cap irregularities (can be transported over long distances)

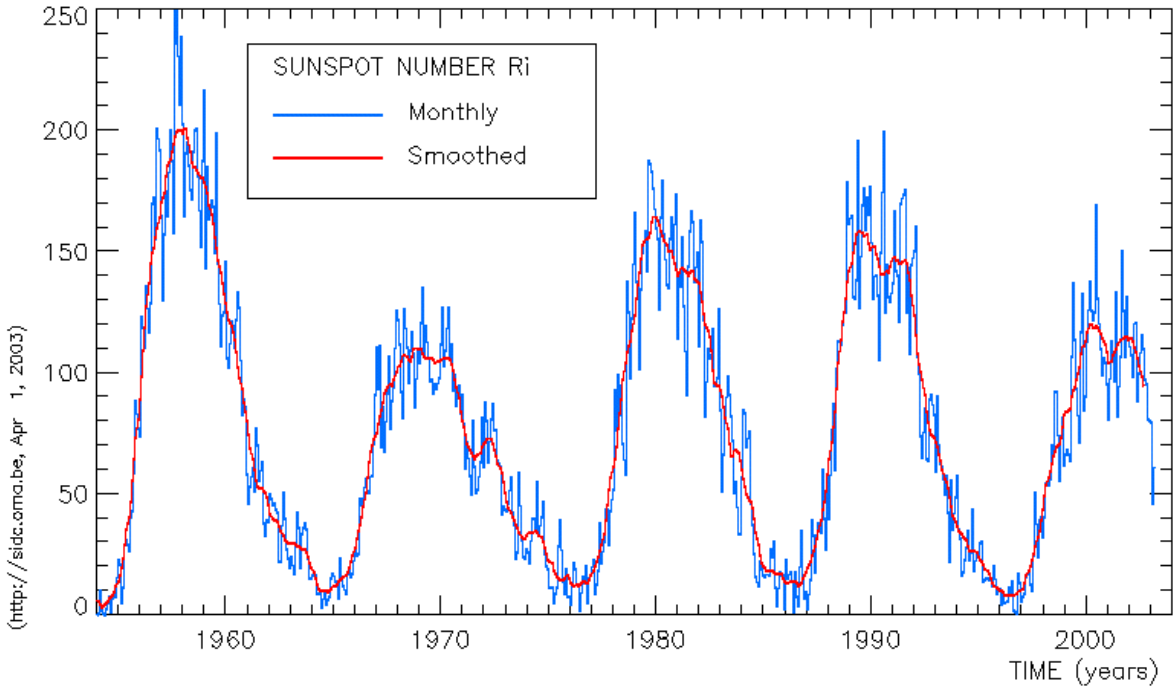

Figure 4.1. The recent solar cycles represented by variation of sunspot number.

The solar cycle variation essentially effects the ionosphere through two different mechanisms. On the one hand there is a gradually change in the short wavelength solar spectrum which peaks at sunspot maximum. Since this part of the spectrum reacts strongly with the neutral atmosphere the ionospheric production rate varies throughout the solar cycle. This effect is incorporated in the IRI-2000 model, and was consequently taken into account in table 3.1. However, the sun also emits a thin plasma called the solar wind at all times as well as more

high energetic charged particles at intermittent intervals. In turn these effects gives rise to three main components of ionospheric disturbances at high latitudes. These are the auroral particle precipitation, polar cap irregularities and polar cap absorption events. The intensity and frequency of variations in these processes also increases with sunspot number, but they are not dealt with in the IRI-2000 model. However, the main effects will be briefly summarised in the following.

4.1 Aurora and particle precipitation

The aurora is caused mainly by precipitating electrons in the energy range 1–10 keV. The electrons are accelerated by processes in near-Earth space which are ultimately influenced by solar wind variations. In addition to producing the auroral emissions, these electrons also causes increased ionisation at altitudes ranging from 100 km to 300 km. The precipitation occurs in an oval centred around the geomagnetic poles, which due to the offset of the Earth's magnetic dipole axis from the rotation axis, are displaced considerably from the geographic poles.

The statistical location of the auroral oval is dependent on geomagnetic activity as illustrated in figure 4.2 below. The upper panel shows the location of the oval at geomagnetically quiet times, while the lower panel shows the corresponding location during geomagnetically disturbed periods. In this view the oval is seen from above with the sun located off the left hand side of the panel. As is seen, the auroral oval covers large parts of Norway at nightime during disturbed conditions. The precipitation along the oval is highly varying in terms of energy and intensity, but the most intense and frequent precipitation in any part of the oval will occur near local magnetic midnight (at Andøya this corresponds to about 22 local time).

Historically the visible auroral activity has been summarised in the q-index, ranging from q=1 (quiet times) to q=6 (very disturbed). This corresponds to the same activity range as the more widely known Kp-index for measuring geomagnetic activity. This index ranges from Kp = 1 (quiet times) to Kp= 9 (very disturbed). The Kp-index is derived from measurements obtained at various magnetic observatories around the world, and it is available on the web. In fact, quite good predictions of the Kp-index for the upcoming three hour period are also available on the web.

We have studied the effects of strong aurora and particle precipitation on the wave propagation and we find that, using the four profiles given in Section 3.2, the uncertainty in deriving the position of a transmitter is less than 1 m in all cases. This is regarded as insignificant.

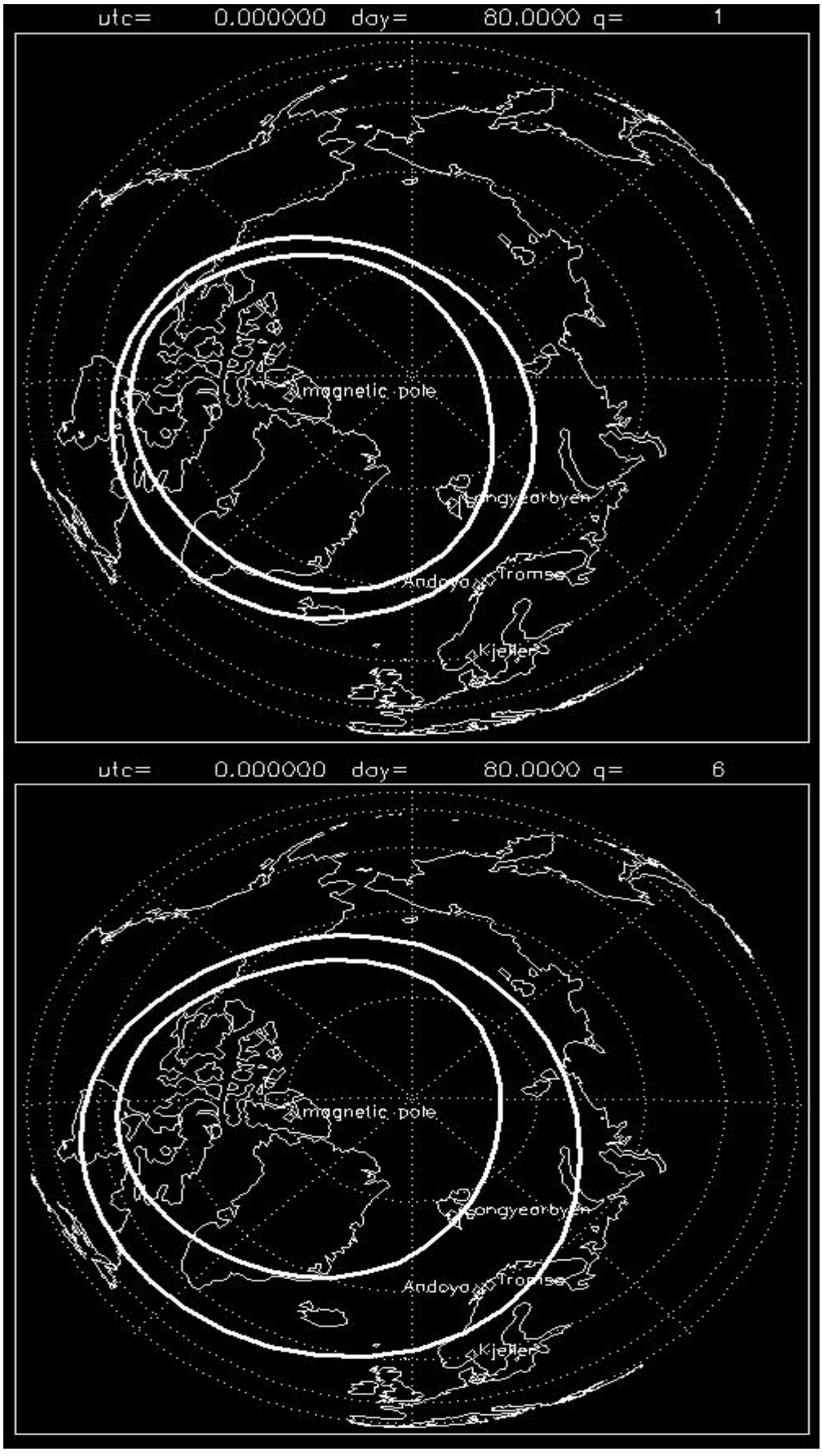

Figure 4.2. The auroral oval at geomagnetic quiet times (top) and disturbed times (bottom).

4.2 Polar cap irregularities

Polar cap irregularities can occur either in the F-layer or in the E-layer. They are usually associated with transpolar arcs (theta aurora) or "blobs" of plasma which are transported by convection (anti-sunwards across the polar cap and sunwards along the oval). The plasma blobs consist of regions of increased electron density and temperature, but their origin is not unambiguously determined as yet. Both dayside particle precipitation, as well as the influx of plasma from low latitudes due to geomagnetic field variations, are at present considered likely sources. In any case, both of these mechanisms are more active at time of high geomagnetic activity. Hence, polar cap irregularities are also more prevalent at solar maximum.

The most conspicuous effect of these irregularities is to cause scintillations in the signal path. Such scintillations in turn lead to fading of the signal strength, and it is as such an additional damping term in the transmission budget. Figure 4.3 shows where scintillations are commonly observed at L-band (~1.5 GHz – close to GPS). Scintillations are often observed in the polar cap, but more frequently at times when the interplanetary field is directed southward. Since such a state also more frequently leads to geomagnetic activity, scintillations are also more frequent during disturbed geomagnetic conditions. As a consequence, scintillations occur more often at solar maximum.

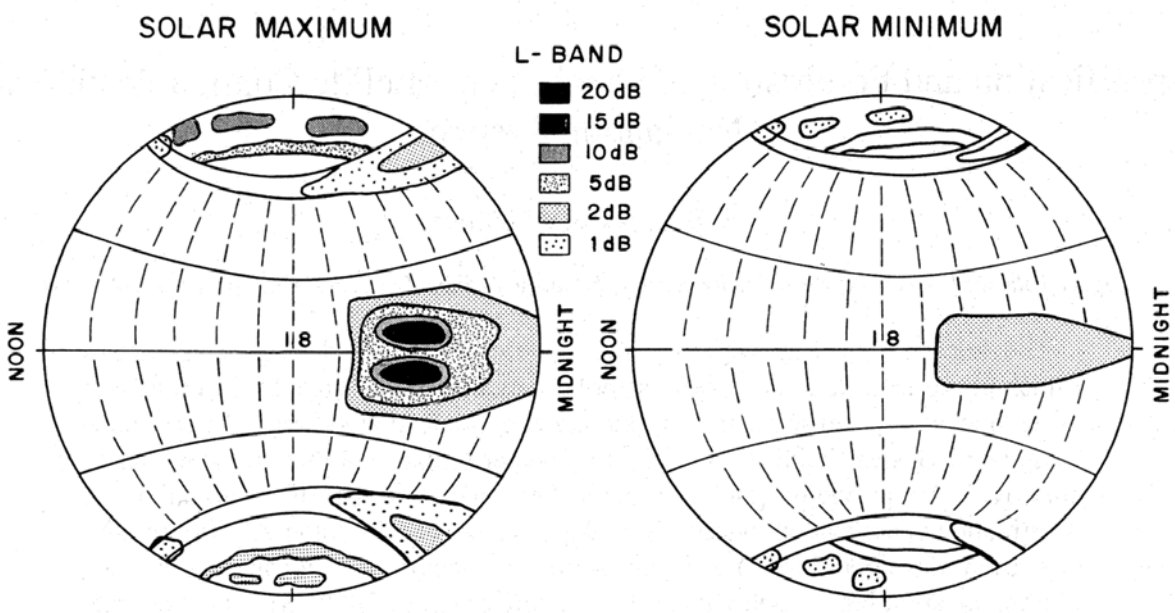

Figure 4.3. The occurrence of L-band scintillations as measured by signal fading. It is seen that additional signal damping of 10 dB or so may occur over the polar cap due to local plasma irregularities. This form of damping is most severe at solar maximum (Basu et al., 2002).

However, it is clear that the effect of polar cap irregularities is strongly frequency dependent as is illustrated in figure 4.4 below. Scintillations are here measured at three different frequencies

at 257 MHz, 1541 MHz and 3954 MHz (data recorded at Ascension Island at solar maximum). It is seen that the effects in the form of signal fading are already very small in the latter case.

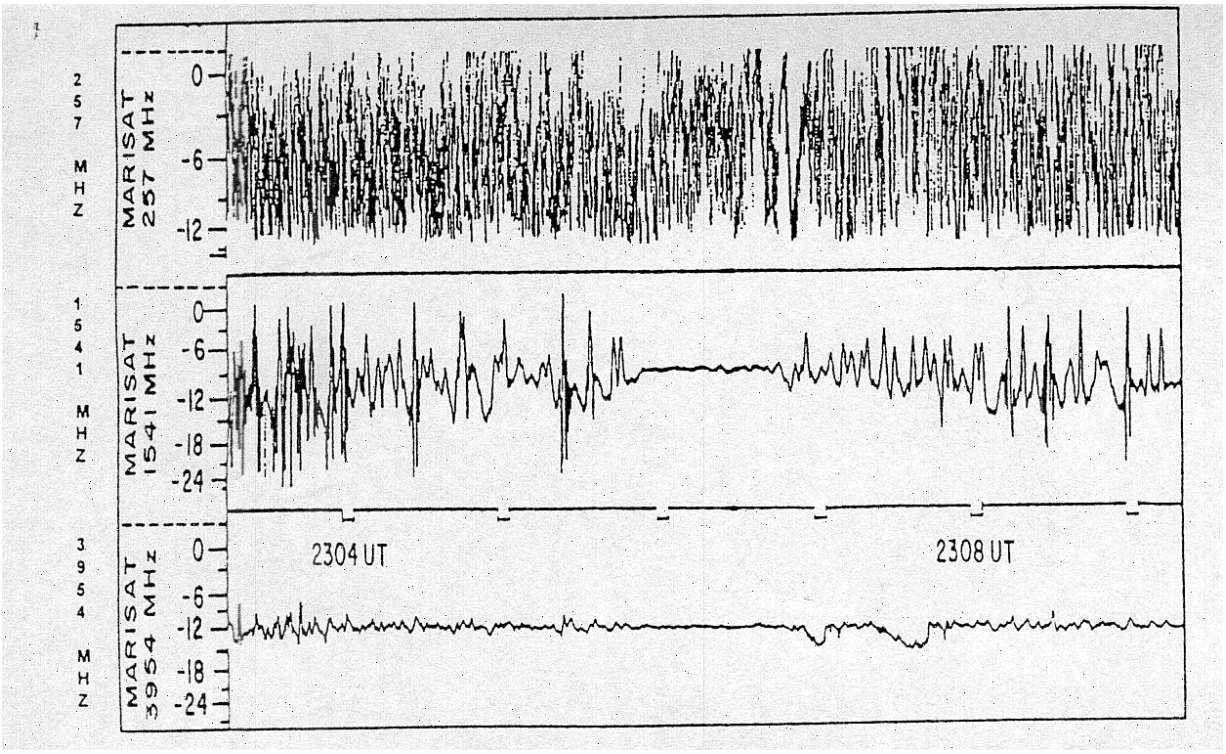

Figure 4.4. Scintillation measured as a function of frequency at 257 MHz (top panel), 1541 MHz (middle panel) and 3954 MHz (bottom panel) (Basu et al., 2002).

Consequently, it is anticipated that signal fading due to polar cap irregularities will only cause minor effects in the frequency range applicable in the NSAT-1 project.

4.3 Polar Cap Absorption events (PCA)

Polar cap absorption events are cause by the arrival of energetic protons of solar origin. The proton populations are caused by eruptive events at the sun, and they have energies in the MeV range. Such solar eruptions are somewhat more frequent during solar maximum. These events are in any case fairly rare, occurring on the order of once every month, but the effects in the ionosphere can last for days.

However, as the particle spectrum is very energetic, they consequently create only an additional ionisation layer at D-region altitudes. We have, as for the auroral cases, determined the effect of a typical PCA-event. We again find that the effect is less than 1 m in geolocation uncertainty, and consequently PCA-events insignificant in the NSAT-1 project.

5 SUMMARY AND CONCLUSIONS

We have in this report studied the effects of the ionosphere upon radio-wave transmission in the X-band. We have studied solar cycle effects, winter and summer conditions, as well as various ionospheric disturbances, e.g. aurora and polar cap absorption. We have studied both the uncertainty in deriving the position of a transmitter on the ground as well as possible polarization effects. We have reached the following two basic conclusions:

1. The error (deviation) in determining the position of a transmitter on the ground is for all practical purposes less than 50 m in all cases considered, as long as the nadir angle is smaller than 65°.

2. The phase of the wave changes by less than 0.03° between the transmitter and the receiver.

References

(1) Basu, S., K.M. Groves, Su. Basu, P.J. Sultan (2002): Specification and forecasting of scintillations in communication/navigation links: current status and future plans, *Journ.Atmos.Solar-Terr.Phys.* **64**, 1745-1754.

(2) Schlüter, S., N. Jakowski, S. Heise (2002): Assessment of ionosphere parameter and correction models, Technical Note ID 23/25a.3, Is. 2, German Aerospace Centre, Institute of Communications and Navigation, D-17235 Neustrelitz, Germany.

(3) Hoppe, U.-P. (2002): GALILEOSAT SYSTEM TEST BED - Første prosjektmøte, FFI/REISERAPPORT-2002/02408, Unntatt offentlighet §5.1

(4) Ofstad, A.E., Ø. Berggraf, V. Odden, K.D. Mildal, U.-P. Hoppe, T.L. Hansen (1991): GPS in Actic Areas II, Report No. GEO 91-10, Norwegian Hydrographic Service.

(5) Bilitza, D (2001): International Reference Ionosphere 2000, *Radio Science* **36**, 2, 261-275.

DISTRIBUTION LIST

FFIE **Dato:** 23. mai 2003

RAPPORTTYPE (KRYSS AV)	RAPPORT NR.	REFERANSE	RAPPORTENS DATO
X RAPP ☐ NOTAT ☐ RR	2003/01761	FFIE/416/172	23. mai 2003
RAPPORTENS BESKYTTELSESGRAD		ANTALL TRYKTE UTSTEDT	ANTALL SIDER
Unclassified		25	23
RAPPORTENS TITTEL		FORFATTER(E)	
IONOSPHERIC INFLUENCE ON X-BAND RADIO SIGNALS		BLIX Tom Arild, SVENES Knut Ragnar, HOPPE Ulf-Peter	
FORDELING GODKJENT AV FORSKNINGSSJEF		FORDELING GODKJENT AV AVDELINGSSJEF:	
Vidar S Andersen		Johnny Bardal	

EKSTERN FORDELING

ANTALL	EKS NR	TIL

INTERN FORDELING

ANTALL	EKS NR	TIL
9		FFI-Bibl
1		FFI-ledelse
1		FFIE
1		FFISYS
1		FFIBM
1		FFIN
1		Tom A Blix
1		Torkild Eriksen, FFIE
1		Ulf-Peter Hoppe, FFIE
1		Gudrun K Høye, FFIE
1		Bente Jensløkken Meland, FFIE
1		Bjørn T Narheim, FFIE
1		Knut R Svenes, FFIE
4		Restopplag til Biblioteket
		Elektronisk fordeling:
		Vidar S Andersen (VSA)
		Vegard Arneson (VAr)
		Jan Hammerstad (JAH)
		Svein Haavik (SvH)
		Vivianne Jodalen (VJo)
		Ørnulf Kandola (OrK)
		Morten Mjanger (MMj)
		Richard Olsen (ROl)
		Bendik Sagsveen (BAS)
		Tore Smestad (TSm)
		Rune Sundgot (Rsu)
		Terje Wahl (TeW)
		Hans Øhra (HOh)
		FFI-veven

Benytt ny side om nødvendig.